Applied Physics Letters

Synchrotron-based analysis of chromium distributions in multicrystalline silicon for solar cells

Cite as: Appl. Phys. Lett. **106**, 202104 (2015); https://doi.org/10.1063/1.4921619
Submitted: 10 April 2015 . Accepted: 05 May 2015 . Published Online: 20 May 2015

Mallory Ann Jensen, Jasmin Hofstetter, Ashley E. Morishige, Gianluca Coletti, Barry Lai, David P. Fenning, and Tonio Buonassisi

Synchrotron-based analysis of chromium distributions in multicrystalline silicon for solar cells

Mallory Ann Jensen,[1,a)] Jasmin Hofstetter,[1,b)] Ashley E. Morishige,[1] Gianluca Coletti,[2] Barry Lai,[3] David P. Fenning,[1,4] and Tonio Buonassisi[1,c)]
[1]*Massachusetts Institute of Technology, Cambridge, Massachusetts 02139, USA*
[2]*ECN Solar Energy, Westerduinweg 3, NL-1755 LE Petten, The Netherlands*
[3]*Advanced Photon Source, Argonne National Laboratory, Argonne, Illinois 60439, USA*
[4]*University of California, San Diego, La Jolla, California 92093, USA*

(Received 10 April 2015; accepted 5 May 2015; published online 20 May 2015)

Chromium (Cr) can degrade silicon wafer-based solar cell efficiencies at concentrations as low as $10^{10}\,cm^{-3}$. In this contribution, we employ synchrotron-based X-ray fluorescence microscopy to study chromium distributions in multicrystalline silicon in as-grown material and after phosphorous diffusion. We complement quantified precipitate size and spatial distribution with interstitial Cr concentration and minority carrier lifetime measurements to provide insight into chromium gettering kinetics and offer suggestions for minimizing the device impacts of chromium. We observe that Cr-rich precipitates in as-grown material are generally smaller than iron-rich precipitates and that Cr_i point defects account for only one-half of the total Cr in the as-grown material. This observation is consistent with previous hypotheses that Cr transport and $CrSi_2$ growth are more strongly diffusion-limited during ingot cooling. We apply two phosphorous diffusion gettering profiles that both increase minority carrier lifetime by two orders of magnitude and reduce $[Cr_i]$ by three orders of magnitude to $\approx 10^{10}\,cm^{-3}$. Some Cr-rich precipitates persist after both processes, and locally high $[Cr_i]$ after the high-temperature process indicates that further optimization of the chromium gettering profile is possible. © *2015 AIP Publishing LLC*. [http://dx.doi.org/10.1063/1.4921619]

Chromium (Cr) is a detrimental impurity in silicon, impacting solar cell performance at concentrations as low as $10^{10}\,cm^{-3}$.[1–3] Chromium is a major component of stainless steel, which is often used in wafer-fabrication equipment. Metal impurities such as chromium, especially when present as interstitial or substitutional point defects, act as minority-carrier recombination centers, limiting charge-carrier lifetimes at device-relevant excess-carrier densities.[4,5] Interstitial chromium (Cr_i) is highly effective at capturing minority carriers: the capture cross-sections for chromium are 1.5 and 57 times larger than iron in *p*- and *n*-type silicon, respectively.[2]

Knowledge of the thermodynamics and kinetics of a contaminant can inform diffusion gettering profile design to mitigate the impurity impact on solar cell efficiency. Iron, for example, has been well-studied, and kinetics process simulation tools exist to engineer its distribution in the material.[6–9,33] The impact of processing steps on chromium (both precipitated and interstitial) has not been studied as extensively, although the detrimental nature of the impurity is well-known. The maximum allowable chromium contamination in the silicon melt ranges from $1 \times 10^{15}\,cm^{-3}$ to $2 \times 10^{17}\,cm^{-3}$ depending on the growth process, device architecture, and target efficiency.[3,10,11]

The distribution and chemical state of an impurity are essential inputs to kinetics process simulations. Formation of chromium disilicide ($CrSi_2$) precipitates during crystallization has been confirmed by energy dispersive X-ray spectroscopy.[12] Given a high concentration of chromium, precipitation during cool-down at dislocations in multicrystalline silicon (mc-Si) material after crystallization was predicted by numerical simulation[13] and implied by micro-photoluminescence techniques.[14] Schön *et al*. found that minority carrier lifetime increased and $[Cr_i]$ decreased after phosphorous diffusion gettering.[13] Other quantitative studies of the effect of phosphorous diffusion gettering have measured high chromium concentrations at near-surface regions, suggesting external gettering,[15–17] as well as a reduction of the total bulk chromium concentration.[18]

For this study, two adjacent (sister) wafers were selected from a 12 kg laboratory-scale intentionally chromium-contaminated mc-Si ingot.[11] These wafers were taken from 83% ingot height. From boron (B) and Cr concentrations of 0.34 ppma and 108 ppma added to the melt, we estimate a *p*-type B doping concentration of $1.9 \times 10^{16}\,cm^{-3}$ and a Cr concentration of $9.9 \times 10^{13}\,cm^{-3}$ using the Scheil equation. Segregation coefficients for B and Cr were taken to be 0.8[19] and 3.1×10^{-6},[11] respectively. The estimated B concentration is consistent with resistivity measurements. For synchrotron-based micro-X-ray fluorescence (μ-XRF) measurements, 1 cm^2 samples were cut from vertically adjacent locations in the wafers. Electron backscatter diffraction (EBSD) was used to identify a random angle grain boundary (35.3°) for analysis. Prior to measurements, the as-grown samples were saw-damage etched (CP4) and RCA-cleaned; for post-gettering measurements, the phosphorous silicate glass (PSG) layer was etched with HF and samples were RCA-cleaned, leaving the phosphorous-doped emitter layer intact. In each state (as-grown and post-gettering), spatially

a)Electronic mail: mal.ann.jensen@gmail.com
b)Present address: 1366 Technologies, Bedford, Massachusetts 01730, USA.
c)Electronic mail: buonassisi@mit.edu

resolved μ-XRF measurements were taken in the same location along at least 20 μm of the aforementioned grain boundary, with a step size of 220 nm and a full-width half-maximum beam spot size of approximately 200 nm. μ-XRF measurements were conducted at the Advanced Photon Source beamline 2-ID-D at Argonne National Laboratory. μ-XRF data analysis assumes a spherical $CrSi_2$ precipitate with a unit cell volume of 3.61×10^{-23} cm^3.[20,21] The μ-XRF measurement and analysis procedure are outlined, in detail, in Ref. 8; a noise cutoff of four standard deviations was used to process the data presented herein.

Three 5×4 cm^2 samples were cut from each sister wafer for lifetime and chromium point-defect concentration measurements. After saw-damage (as-grown) and emitter (post-gettering) removal by CP4 followed by RCA cleaning, a 20 nm passivating layer of Al_2O_3 was deposited on both sides of the samples by atomic layer deposition (ALD) at 200 °C (Cambridge NanoTech Savannah 200) followed by a 12-min anneal in a N_2 ambient at 350 °C. Spatially resolved lifetime and chromium point-defect concentrations (post-gettering) were measured by performing a series of photoconductance-calibrated photoluminescence (PC-PL) measurements in isolated defect states, as described in Refs. 22 and 23. First, the sample was heated in the dark at 250 °C for 10 min and then illuminated at room temperature for 1 min with an 808 nm diode laser (Lumics, 25 W, operated at 70% power, ≈0.25 suns) to dissociate iron-boron (Fe_i-B_s) pairs just before a lifetime measurement was performed (Cr_i, Fe_i, and BO-complex largely deactivated). A second thermal dissociation at 250 °C in the dark for 10 min was applied before storing in the dark at 70 °C for 5 h. Thereafter, the sample was illuminated for 1 min to dissociate Fe_i-B_s pairs and the second lifetime measurement was performed (Cr_i-B_s, Fe_i, and BO-complex largely deactivated). Equations (1)–(10) and Shockley-Read-Hall defect parameters reported in Ref. 22 were used to calculate [Cr_i]. The Cr_i donor level lies at 0.24 eV below the conduction band in silicon, with an electron-to-hole capture cross-section asymmetry k equal to 5.[22] The Cr_i-B_s defect complex is dominant in B-doped p-type silicon with a donor level 0.27 eV above the valence band and a k value of 2. Average lifetime and chromium point-defect concentrations (as-grown and post-gettering) were also measured in a similar manner with a Sinton Instruments WCT-120.

All PL measurements were performed using the 808 nm diode laser and a Princeton Instruments PIXIS 1024BR camera, fitted with an InP wafer and a Schott RG1000 long-pass filter. The WCT-120 was used to calibrate the PL images according to Ref. 24. A Czochralski silicon sample of similar thickness, reflectivity, and resistivity was used to determine the calibration parameters. We corrected the second fit parameter (b in $y = ax^2 + bx$), proportional to the doping concentration of the sample,[24] to match the chromium sample doping concentration. The PL measurement variation is 4.4%, estimated by imaging the Czochralski sample 15 times while illuminated under similar conditions. The detection limit (≈5×10^9 cm^{-3} in the highest lifetime areas) is estimated pixel-by-pixel by propagating this uncertainty through the [Cr_i] calculation.

The samples were subjected to phosphorous diffusion gettering in a $POCl_3$ tube furnace (Tystar Titan 3800). The samples from the first sister wafer received a standard diffusion (STD): annealed at 845 °C for 25 min and unloaded directly at 845 °C. The samples from the second sister wafer received a high-temperature extended diffusion (EXT): annealed at 920 °C for 76 min, and cooled to 600 °C for an additional 60 min anneal before unloading. The EXT process was chosen due to its enhanced iron gettering efficiency compared to the STD process.[9]

In the as-grown state, chromium precipitates were detected by μ-XRF along the random-angle grain boundary (Fig. 1), consistent with the behavior of other metals in silicon wherein metal precipitate nucleation is favored at bulk heterogeneous nucleation sites.[25–27] A total of 18 precipitates were measured with a precipitate line density of 0.42 precipitates/μm. These Cr-rich precipitates in the as-grown material were found to be co-located with copper-rich particles and to be smaller on average than iron-rich precipitates formed under similar crystallization conditions in another ingot (Fig. 2). In the iron-contaminated material presented in Ref. 8 ([Fe] = 5.0×10^{14} cm^{-3}), a total of 30 iron-rich precipitates were identified, with a line density along a Σ3 grain boundary equal to 1.27 precipitates/μm. The iron and chromium as-grown precipitate size distributions are compared in Fig. 2. The noise floors, represented by the gray "+" for each distribution, are similar in magnitude. Due to the high detection limits, the precipitate distributions cannot be fully specified by μ-XRF data.[28] No chromium precipitate larger than 3.6×10^5 Cr atoms/precipitate is detected, while the maximum iron precipitate size is nearly one order of magnitude larger, 2.9×10^6 Fe atoms/precipitate. Similar differences in precipitate size after crystallization were predicted through simulation by Schön *et al.*[13] The authors attributed the tendency toward smaller chromium precipitates to a lower diffusivity of chromium compared to iron. We confirm their conclusions, noting that, in our comparison, the iron contamination level is slightly higher than the chromium contamination level.

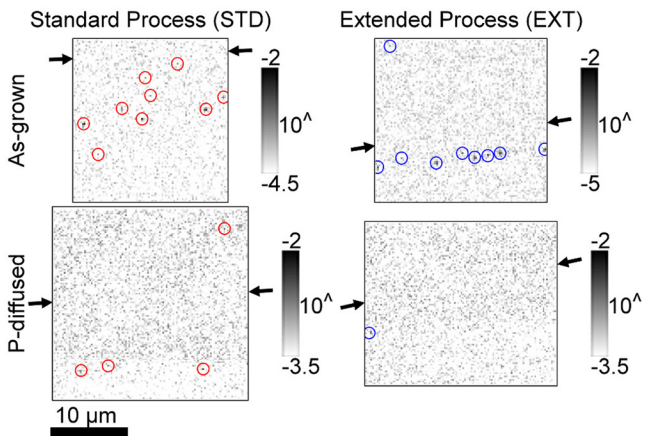

FIG. 1. Representative as-grown and gettered synchrotron measurements of intentionally contaminated sister samples. In each spatially resolved map, the pixel intensity is determined by the fluorescence associated with chromium, measured in μg/cm^2 with a logarithmic scale. Precipitates identified to be above the estimated noise floor are circled in red (STD) and blue (EXT). These images have been cropped for display, while the analysis in Fig. 2 has been performed on the full data set. Black arrows indicate where the grain boundary line (visible from elastically scattered X-rays, not shown) enters and exits the map.

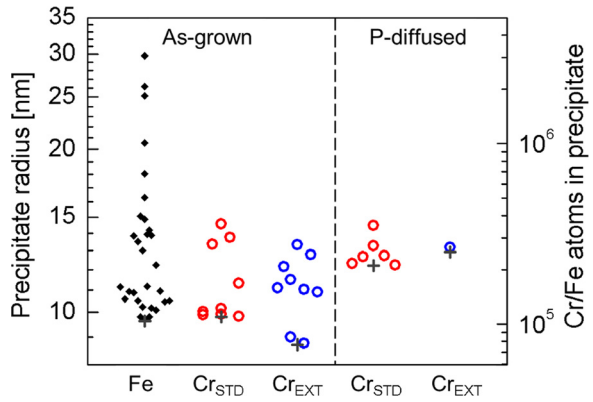

FIG. 2. Precipitate distributions obtained from automated analysis of the spatially resolved maps for iron (reported in Ref. 8) and chromium (this study). The gray "+" on each distribution represents the estimated noise floor of the measurement.

Process	Lifetime [μs]	Chromium [cm^{-3}]
As-grown	0.18 ± 0.04	(4.5 ± 0.8)×10^{13}
STD	15.0 ± 3.2	(2.3 ± 0.6)×10^{10}
EXT	25.7 ± 14.4	(3.1 ± 1.2)×10^{10}

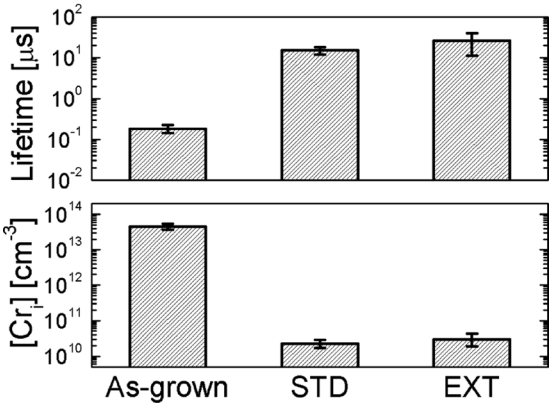

FIG. 3. Average lifetime at $\Delta n = 10^{15}\,\mathrm{cm}^{-3}$ (middle) and $[Cr_i]$ (bottom) for three samples in each process state. Error bars represent the standard deviations of the measurements.

After phosphorous diffusion, some Cr-rich precipitates remain (Figs. 1 and 2), while the co-located copper fluorescence is no longer detectable. This suggests that the phosphorus diffusion processes were insufficient to getter all precipitated metals, especially Cr, consistent with the Cr solubility estimates at the different temperatures ($1.46 \times 10^{12}\,\mathrm{cm}^{-3}$ at 845 °C and $9.01 \times 10^{12}\,\mathrm{cm}^{-3}$ at 920 °C). After the STD process, six particles are identified, while after the EXT process, one particle is identified. Quantitative comparisons between as-grown and phosphorus-diffused states are challenging because a small number of precipitates are identified and the μ-XRF background signal is higher for the phosphorus-diffused than for the as-grown measurements. The change in background level is due to differences in measurement setup, likely the distance between the detector and the sample, confirmed by corresponding μ-XRF measurements of NIST standard reference material 1832.

Analysis of the larger samples suggests that $[Cr_i]$ is decreased by phosphorous diffusion, confirming previous observations.[13,15–18] Lifetimes (Cr_i, $\Delta n = 10^{15}\,\mathrm{cm}^{-3}$) and interstitial concentrations as measured by quasi-steady-state photoconductance (QSSPC) before and after gettering are shown in Fig. 3. For each sample, the chromium concentration is taken to be the median value across the full range of measured injection levels, excluding trapping regimes. Calculated chromium concentrations requiring less than 1% measurement precision based on the lifetime and injection level are excluded. The as-grown interstitial concentration constitutes roughly one-half of the total estimated chromium concentration, with the remaining chromium assumed to be in precipitated form as observed by μ-XRF. Both time-temperature profiles result in average lifetime increases from 0.1 to at least 10 μs and $[Cr_i]$ reductions from 10^{13} to $10^{10}\,\mathrm{cm}^{-3}$. In the as-grown state, the Cr_i-limited Shockley-Read-Hall lifetime at $10^{15}\,\mathrm{cm}^{-3}$ injection is 0.2 μs; post-gettering, the Cr_i-limited lifetimes are 413 and 309 μs for STD and EXT, respectively. The effective lifetimes measured post-gettering are significantly lower than the theoretical Cr-limited lifetimes, though some of the lifetime improvement should be attributed to gettering of iron and/or other impurities. Our results therefore indicate that, similar to iron, the distribution of chromium can be engineered through gettering. When precipitates are in close proximity (i.e., near a grain boundary), chromium may be internally gettered to existing precipitates, allowing them to retain their sizes after processing. The remaining chromium ($\approx 10^{13}\,\mathrm{cm}^{-3}$ assuming no change in precipitate size or density) is likely externally gettered, diffusing to the emitter and PSG layer as has been observed by SIMS.[15–17] With one-half of the total Cr concentration in precipitated form, a diffusion temperature of ≈990 °C (Cr solubility equal to $4 \times 10^{13}\,\mathrm{cm}^{-3}$) would be required to fully dissolve precipitates.

We find that both the STD and EXT processes are, on average, effective at externally gettering chromium to reduce the total concentration. No consistent difference in final lifetime or $[Cr_i]$ between the two processes is observed (Fig. 3). However, upon closer inspection, the $[Cr_i]$ distributions after the two processes are non-uniform within the wafers. This is seen in Fig. 4(b), which features a representative pair of sister samples with both regions of comparatively lower $[Cr_i]$ after STD and lower $[Cr_i]$ after EXT. In these images, concentrations lower than the pixel-by-pixel calculated detection limit are replaced with a singular low value and appear white. As-grown lifetime images (Fig. 4(a)) display low lifetime overall with higher lifetime denuded zones at grain boundaries.

To evaluate the effect of the two processes on these different regions, we define three areas for comparison. Area 1 (blue circles) contains a large grain of low dislocation density surrounded by other regions of low dislocation density. Lifetime is higher in this area after the EXT compared to the STD process, in which $[Cr_i]$ is near the detection limit. Area 2 (green circles) contains medium dislocation density regions, in which lifetime is higher and $[Cr_i]$ is lower after the EXT process compared to the STD process. Area 3 (red circles) contains high dislocation density regions with higher lifetime and $[Cr_i]$ after the EXT process. Our PL setup does not include corrections for lateral carrier diffusion due to inhomogeneous excess carrier densities,[23,29] photon scattering or reabsorption within the sample,[30] or photon spreading within the sensor,[31,32] all of which may impact the spatial

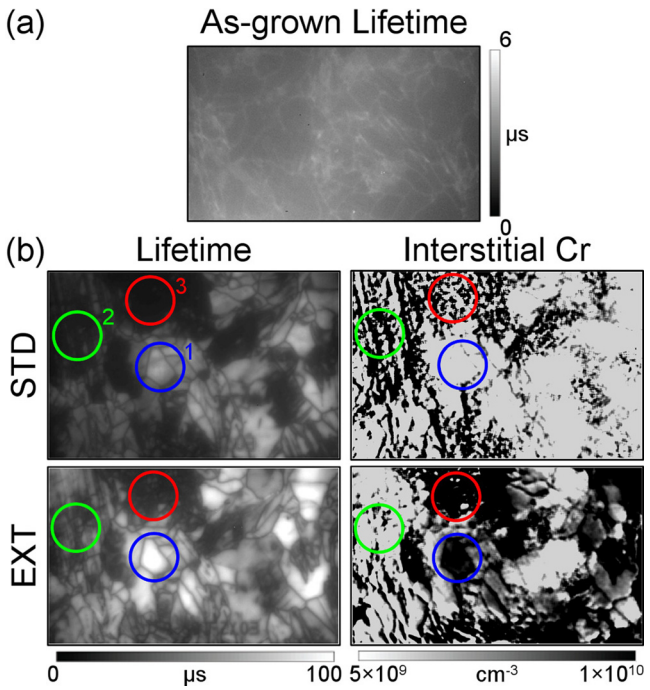

FIG. 4. (a) Spatially resolved lifetime of a representative sample in the as-grown state. (b) Lifetime and [Cr_i] maps of two representative adjacent wafers, one subjected to the standard process (STD) and one subjected to the extended process (EXT). In the lifetime images, dark areas correspond to low lifetime and light areas correspond to high lifetime. In the [Cr_i] images, dark areas correspond to high concentrations and light areas correspond to low concentrations on a logarithmic scale. The solid blue, green, and red circles were selected to compare the two different gettering processes.

information especially in inhomogeneous areas. The setup was constant for all measurements; the trends in [Cr_i] are therefore conserved but we acknowledge the possibility of measurement artifacts in Areas 2 and 3.

The results in each area can be explained by considering that the higher temperature EXT process may more effectively dissolve small Cr-rich precipitates. In areas of low dislocation density (Area 1), Cr_i atoms may be "frozen" into bulk intragranular regions during cooling. Combined with a reduction in other impurity concentrations during gettering, the remaining Cr_i ($\approx 10^{10}\,cm^{-3}$) in these intragranular, high-lifetime regions can contribute significantly to the local performance (≈20% of the total recombination rate due to Cr_i after EXT). In contrast, areas of medium and high dislocation density may differ in as-grown precipitate density due to differences in the density of heterogeneous nucleation sites. In Area 2, the EXT process appears to be sufficient and preferable to the STD process to dissolve precipitates and externally getter Cr. In Area 3, the EXT process results in frozen Cr_i atoms, but due to low lifetime presumably limited by structural defects, the Cr_i contribution to the recombination rate remains less than 5% after both processes. Therefore, although both processes are effective at externally gettering and reducing the total concentration of Cr, the spatially resolved results after the EXT process in particular indicate that there are some areas of incomplete external gettering which require a higher temperature and/or longer duration anneal.

In summary, μ-XRF, lifetime, and [Cr_i] measurements were used to quantify the as-grown distributions and gettering response of precipitated and interstitial chromium in mc-Si. We confirm the smaller size of as-grown Cr-rich precipitates compared to iron-rich precipitates, consistent with diffusion-limited precipitation. After phosphorous diffusion gettering, we conclude that some Cr was externally gettered, but due to the high initial concentration and the existence of Cr-rich precipitates, the gettering processes tested were not sufficient for complete removal of chromium. An even higher diffusion temperature is required to dissolve all precipitates (estimated ≈990 °C in this case). To prevent localized lifetime degradation due to Cr_i, an annealing step should be implemented with sufficient temperature and time to allow for complete external gettering after cooling.

We thank D. M. Powell, S. Castellanos, and M. Kivambe for experimental support and mentorship. We thank I. M. Peters, C. del Cañizo, H. Wagner, J. Schön, G. Hahn, J. Tan, and F. Fertig for insightful discussions regarding experiments, data analysis, and manuscript preparation. This work was supported by the U.S. Department of Energy (DOE) under Contract No. DE-EE0005314, and by the National Science Foundation (NSF) and the DOE under NSF CA No. EEC-1041895. M. A. Jensen acknowledges support by the National Science Foundation Graduate Research Fellowship under Grant No. 1122374, and A. E. Morishige acknowledges the support of the Department of Defense through the National Defense Science and Engineering Graduate Fellowship Program. EBSD and ALD were performed at the Center for Nanoscale Systems (CNS), a member of the National Nanotechnology Infrastructure Network (NNIN), which is supported by the National Science Foundation under NSF Award No. ECS-0335765. μ-XRF was performed at the Advanced Photon Source, a U.S. Department of Energy (DOE) Office of Science User Facility operated for the DOE Office of Science by Argonne National Laboratory under Contract No. DE-AC02-06CH11357.

[1]J. R. Davis, A. Rohatgi, R. H. Hopkins, P. D. Blais, P. Rai-Choudhury, J. R. McCormick, and H. C. Mollenkopf, "Impurities in silicon solar cells," IEEE Trans. Electron Devices **27**(4), 677–687 (1980).
[2]J. Schmidt, B. Lim, D. Walter, K. Bothe, S. Gatz, T. Dullweber, and P. P. Altermatt, "Impurity-related limitations of next-generation industrial silicon solar cells," IEEE J. Photovoltaics **3**(1), 114–118 (2013).
[3]G. Coletti, "Sensitivity of state-of-the-art and high efficiency crystalline silicon solar cells to metal impurities," Prog. Photovoltaics Res. Appl. **21**(5), 1163–1170 (2013).
[4]W. Shockley and W. T. Read, "Statistics of the recombinations of holes and electrons," Phys. Rev. **87**(5), 835–842 (1952).
[5]R. N. Hall, "Electron-hole recombination in germanium," Phys. Rev. **87**(2), 287 (1952).
[6]A. Haarahiltunen, H. Savin, M. Yli-Koski, H. Talvitie, and J. Sinkkonen, "Modeling phosphorus diffusion gettering of iron in single crystal silicon," J. Appl. Phys. **105**(2), 023510 (2009).
[7]J. Hofstetter, D. P. Fenning, M. I. Bertoni, J. F. Lelièvre, C. del Cañizo, and T. Buonassisi, "Impurity-to-efficiency simulator: predictive simulation of silicon solar cell performance based on iron content and distribution," Prog. Photovoltaics Res. Appl. **19**(4), 487–497 (2011).
[8]D. P. Fenning, J. Hofstetter, M. I. Bertoni, G. Coletti, B. Lai, C. del Cañizo, and T. Buonassisi, "Precipitated iron: A limit on gettering efficacy in multicrystalline silicon," J. Appl. Phys. **113**(4), 044521 (2013).
[9]D. P. Fenning, A. S. Zuschlag, J. Hofstetter, A. Frey, M. I. Bertoni, G. Hahn, and T. Buonassisi, "Investigation of lifetime-limiting defects after high-temperature phosphorus diffusion in high-iron-content multicrystalline silicon," IEEE J. Photovoltaics **4**(3), 866–873 (2014).
[10]J. Hofstetter, J. F. Lelièvre, C. del Cañizo, and A. Luque, "Acceptable contamination levels in solar grade silicon: From feedstock to solar cell," Mater. Sci. Eng., B **159–160**, 299–304 (2009).

[11]G. Coletti, P. C. P. Bronsveld, G. Hahn, W. Warta, D. Macdonald, B. Ceccaroli, K. Wambach, N. Le Quang, and J. M. Fernandez, "Impact of metal contamination in silicon solar cells," Adv. Funct. Mater. **21**(5), 879–890 (2011).
[12]J. B. Mohr, S. H. Park, S. N. Schauer, D. K. Schroder, and J. Kalejs, "Physical and electrical investigation of silicide precipitates in EFG polycrystalline silicon intentionally contaminated with chromium," in Proceedings of the 21st IEEE Photovoltaic Specialists Conference (1990), pp. 711–716.
[13]J. Schön, H. Habenicht, W. Warta, and M. C. Schubert, "Chromium distribution in multicrystalline silicon: Comparison of simulations and experiments," Prog. Photovoltaics Res. Appl. **21**(4), 676–680 (2013).
[14]F. D. Heinz, F. Schindler, W. Warta, and M. C. Schubert, "Interstitial chromium in silicon on the micron scale," Energy Procedia **38**, 571–575 (2013).
[15]S. E. Asher, J. P. Kalejs, and B. Bathey, "SIMS analysis of chromium gettering in crystalline silicon," AIP Conf. Proc. **268**, 409–412 (1992).
[16]A. Bentzen, A. Holt, R. Kopecek, G. Stokkan, J. S. Christensen, and B. G. Svensson, "Gettering of transition metal impurities during phosphorus emitter diffusion in multicrystalline silicon solar cell processing," J. Appl. Phys. **99**(9), 093509 (2006).
[17]D. Bouhafs, N. Khelifati, and A. Boucheham, "Optimized temperature in phosphorous diffusion gettering (PDG) setup of chromium transition metal in solar grade multicrystalline silicon P-type wafers," in *Proceedings of the 5th International Advances in Applied Physics and Materials Science Congress and Exhibition* (2015).
[18]D. Macdonald, A. Cuevas, A. Kinomura, and Y. Nakano, "Phosphorus gettering in multicrystalline silicon studied by neutron activation analysis," in *Proceedings of the 29th IEEE Photovoltaic Specialists Conference* (2002), pp. 285–288.
[19]D. Macdonald, A. Cuevas, A. Kinomura, Y. Nakano, and L. J. Geerligs, "Transition-metal profiles in a multicrystalline silicon ingot," J. Appl. Phys. **97**(3), 033523 (2005).
[20]P. Villars and L. D. Calvert, *Pearson's Handbook of Crystallographic Data for Intermetallic Phases* (Metals Park, OH, American Society of Metals, 1985).
[21]F. Chu, M. Lei, S. A. Maloy, J. J. Petrovic, and T. E. Mitchell, "Elastic properties of C40 transition metal disilicides," Acta Mater. **44**(8), 3035–3048 (1996).
[22]H. Habenicht, M. C. Schubert, and W. Warta, "Imaging of chromium point defects in p-type silicon," J. Appl. Phys. **108**(3), 034909 (2010).
[23]M. C. Schubert, H. Habenicht, and W. Warta, "Imaging of metastable defects in silicon," IEEE J. Photovoltaics **1**(2), 168–173 (2011).
[24]S. Herlufsen, J. Schmidt, D. Hinken, K. Bothe, and R. Brendel, "Photoconductance-calibrated photoluminescence lifetime imaging of crystalline silicon," Phys. Status Solidi RRL **2**(6), 245–247 (2008).
[25]T. Buonassisi, A. A. Istratov, M. Heuer, M. A. Marcus, R. Jonczyk, J. Isenberg, B. Lai, Z. Cai, S. Heald, W. Warta, R. Schindler, G. Willeke, and E. R. Weber, "Synchrotron-based investigations of the nature and impact of iron contamination in multicrystalline silicon solar cells," J. Appl. Phys. **97**(7), 074901 (2005).
[26]T. Buonassisi, A. A. Istratov, M. D. Pickett, M. Heuer, J. P. Kalejs, G. Hahn, M. A. Marcus, B. Lai, Z. Cai, S. M. Heald, T. F. Ciszek, R. F. Clark, D. W. Cunningham, A. M. Gabor, R. Jonczyk, S. Narayanan, E. Sauar, and E. R. Weber, "Chemical natures and distributions of metal impurities in multicrystalline silicon materials," Prog. Photovoltaics Res. Appl. **14**(6), 513–531 (2006).
[27]T. Buonassisi, A. A. Istratov, M. D. Pickett, M. A. Marcus, T. F. Ciszek, and E. R. Weber, "Metal precipitation at grain boundaries in silicon: Dependence on grain boundary character and dislocation decoration," Appl. Phys. Lett. **89**(4), 042102 (2006).
[28]J. Schön, A. Haarahiltunen, H. Savin, D. P. Fenning, T. Buonassisi, W. Warta, and M. C. Schubert, "Analyses of the evolution of iron-silicide precipitates in multicrystalline silicon during solar cell processing," IEEE J. Photovoltaics **3**(1), 131–137 (2013).
[29]S. P. Phang, H. C. Sio, and D. Macdonald, "Carrier de-smearing of photoluminescence images on silicon wafers using the continuity equation," Appl. Phys. Lett. **103**(19), 192112 (2013).
[30]P. Würfel, T. Trupke, T. Puzzer, E. Schäffer, W. Warta, and S. W. Glunz, "Diffusion lengths of silicon solar cells from luminescence images," J. Appl. Phys. **101**(12), 123110 (2007).
[31]B. Mitchell, J. W. Weber, D. Walter, D. Macdonald, and T. Trupke, "On the method of photoluminescence spectral intensity ratio imaging of silicon bricks: Advances and limitations," J. Appl. Phys. **112**(6), 063116 (2012).
[32]D. Walter, A. Fell, E. Franklin, D. Macdonald, B. Mitchell, and T. Trupke, "The impact of silicon CCD photon spread on quantitative analyses of luminescence images," IEEE J. Photovoltaics **4**(1), 368–373 (2014).
[33]J. Schön, H. Habenicht, M. C. Schubert, and W. Warta, "Understanding the distribution of iron in multicrystalline silicon after emitter formation: Theoretical model and experiments," J. Appl. Phys. **109**(6), 063717 (2011).